Journal of Catalysis **207,** 101–112 (2002)
doi:10.1006/jcat.2002.3510, available online at http://www.idealibrary.com on IDEAL®

Physicochemical Properties and Catalytic Activity of Cu–NbZSM-5—A Comparative Study with Cu–AlZSM-5

Izabela Sobczak,* Piotr Decyk,* Maria Ziolek,*,[1] Marco Daturi,† Jean-Claude Lavalley,† Larry Kevan,‡ and A. M. Prakash‡

*A. Mickiewicz University, Faculty of Chemistry, Grunwaldzka 6, 60-780 Poznan, Poland; †Laboratoire Catalyse et Spectrochimie, UMR 6506—ISMRA—Université, 6, Boulevard du Maréchal Juin, 14050 Caen Cedex, France; and ‡Department of Chemistry, University of Houston, Houston, Texas 77204-5641

Received October 17, 2001; revised December 19, 2001; accepted December 19, 2001

Aluminosilicate and niobiosilicate ZSM-5 zeolites have been modified by Cu-cation exchange. Structural and physicochemical properties are determined by niobium insertion in the MFI zeolite framework, as shown by TPR, ESR and FTIR investigations. This behavior justifies the different catalytic properties of Cu–NbZSM-5 samples in the NO decomposition with or without the presence of SO_2 in comparison with Cu–AlZSM-5.

Key Words: **MFI zeolites; niobium; copper; NO decomposition; SO_2 poisoning.**

INTRODUCTION

The very high activity of Cu–ZSM-5 zeolites in the decomposition of NO is well known and since its discovery in 1986 (1) it has been widely studied (2–14). It is well documented that the MFI structure is the most efficient support for direct NO decomposition. However, the explanation for this feature is still not clear. One of the questions concerns the nature of Cu-active species. Some authors (15–18) have stressed the role of Cu(I) cations as active centers and others that Cu(II) species were active (19, 20). Moreover, a Cu(II)–Cu(II) dimer formed from Cu–O–Cu was considered an active site as well (21, 22). Recently (23), a proposed scheme for the decomposition of NO on Cu–ZSM-5 has suggested that Cu(I), Cu(II)O^-, and Cu(II) are active toward NO adsorption and yield various copper–NO complexes, such as Cu(II)–NO, Cu(I)–NO, Cu(I)–$(NO)_2$, Cu(I)–NO_2, and Cu(II)–$(NO_2)(NO)^-$. The presence of the above-listed Cu species and complexes with NO was stated on the basis of ESR, ESEM, and FTIR measurements.

The activity of Cu–ZSM-5 in the decomposition of NO is related not only to the nature of Cu species but also to the presence of OH groups and acidity (9). The catalytic activity of Cu–ZSM-5 is also considered in relation to the changes in physical properties of the zeolite, resulting from ion exchange and aluminum content (4, 7, 8, 11, 12, 24–26). Paul and co-workers (9) described the effect of lattice movements on activity in NO decomposition. These movements destabilize nitrates, which act as site blockers in direct NO decomposition on Cu–ZSM-5. Moreover, ionic mobility has been considered. Both effects depend on the Si/Al ratio in aluminosilicate zeolites (the lower the Si/Al ratio, the higher the mobility and the lower the stability). The nature of T atoms in MFI structures should also influence both effects. Therefore, MFI-type zeolites containing niobium instead of aluminum (denoted NbZSM-5) have been applied in this work as a support for copper. The physicochemical properties of these materials have been studied.

The other aspect of the application of NbZSM-5 zeolites as a matrix for copper is connected with earlier results (27) showing that Nb-containing mesoporous molecular sieves (NbMCM-41) exchanged with copper (Cu–NbMCM-41) are resistant to SO_2 poisoning. However, the activity of Cu–NbMCM-41 in the decomposition of NO was not sufficient. Therefore, one could expect that the application of MFI structures containing Nb in the framework for Cu exchange would allow us to obtain a material sufficiently active in NO decomposition and resistant to SO_2 poisoning.

The present study aimed to determine the physicochemical properties of Cu–NbZSM-5 zeolites, their interaction with NO, and their activity in NO decomposition, as well as the effect of sulfation.

EXPERIMENTAL

Catalyst Preparation

Nb-containing ZSM-5 zeolite (denoted NbZSM-5) with Si/Nb = 28 was prepared by two of us (Kevan and Prakash) and its characterization was presented in an earlier paper (28). This material, as well as aluminosilicate ZSM-5 (denoted AlZSM-5) with Si/Al = 31, Ultrazet T1000/I (IChP–Warsaw), was modified via Cu-cation exchange. The ion

[1] To whom correspondence should be addressed. E-mail: ziolek@amu.edu.pl.

0021-9517/02 $35.00

TABLE 1

Composition of the Catalysts Used in This Work

Catalyst	Si/T^a	Cu/T^a	Cu (wt%)	Cu (ex%)
Cu–AlZSM-5-96	31	0.48	1.6	96
Cu–AlZSM-5-120	31	0.60	2.0	120
CuO + AlZSM-5	31	0.50	1.7	—
Cu–NbZSM-5-52	28	0.26	0.9	52
Cu–NbZSM-5-106	28	0.53	1.9	106
CuO + NbZSM-5	28	0.50	1.8	—

[a] T, Al or Nb in the lattice.

exchange was performed using a conventional method, i.e., stirring the solid in an aqueous solution of $Cu(CH_3COO)_2$ (0.2 M, pH 5.5–6). The appropriate weight of the parent zeolites was flooded with the Cu–salt solution in the ratio Cu : Nb(Al) = 1 : 2. After 8 h of stirring at room temperature (RT), the solid was separated from the solution via decantation and the next portion of $Cu(CH_3COO)_2$ solution (Cu : Nb(Al) = 1 : 2) was added. The mixture was stirred again at RT for 8 h and filtrated without washing. The sample with 52% Cu exchange was treated only once with $Cu(CH_3COO)_2$. The obtained samples were calcined at 673 K for 4 h (RT → 673 K, 4 K min^{-1}). Moreover, the mixtures of CuO and NbZSM-5 or AlZSM-5 (Cu : Nb(Al) = 1 : 2) were prepared via mixing in agat moltar.

The catalysts used in this study are presented in Table 1.

H_2 TPR

Temperature-programmed reduction (TPR) of the samples was carried out using H_2/Ar (10 vol%) as reductant (flow rate = 32 cm^3 min^{-1}). The sample (0.04 g) was placed in a quartz tube, treated under a flow of helium at 723 K for 2 h, sulfated with $SO_2 + O_2$ at 673 K for 1 h, treated for 10 min under a He flow at 673 K, and cooled to room temperature. Then it was heated at a rate of 10 K min^{-1} to 1300 K under the reductant mixture. Hydrogen consumption was measured using a thermal conductivity detector in the PulseChemiSorb 2705 (Micromeritics) apparatus.

FTIR Measurements

FTIR spectroscopy was used to characterize Cu species in the catalysts and complexes formed after NO adsorption and decomposition. Infrared spectra were recorded with a Nicolet 710 FTIR spectrometer using an *in situ* cell. The samples were pressed, under low pressure, into wafers (∼12 mg cm^{-2}) and placed in the cell. The catalysts were activated under the following conditions: calcination under pure O_2 at 723 K for 1 h, cooling to RT, evacuation of oxygen at RT, and evacuation at 723 K for 7 h. In some cases the catalysts were further oxidized under an oxygen atmosphere at 723 K for 30 min. The experiments were carried out in three ways: (i) NO adsorption at RT followed by heating to 673 K; (ii) SO_2 adsorption followed by NO admission, heating to 673 K, and evacuation at various temperatures; and (iii) $SO_2 + O_2$ adsorption followed by heating at 673 K, evacuation, and NO admission. All spectra were recorded at room temperature.

Pyridine adsorption on the catalysts was conducted after the activation carried out at the same conditions as before NO adsorption. After saturation the samples were degassed at RT and at 423, 523, 623, and 723 K in vacuum for 30 min.

ESR Study

ESR measurements were conducted after evacuation of the catalyst at various temperatures (RT to 723 K). ESR spectra were recorded at 77 K on a RADIOPAN SE/X 2547 spectrometer. The patterns were obtained at ν_{ESR} = 8.9 GHz. The g value was calculated according to the commonly used equation $g = h\nu/\mu_B B$.

Activity in NO Decomposition

The decomposition of nitric oxide was carried out in a glass flowthrough reactor working at atmospheric pressure. The reaction conditions were as follows: 5% NO in He was passed downward at a total flow rate of 10 cm^3 min^{-1} through the reactor, which contained 0.1 g of ZSM-5 with a grain size of $0.5 < \varnothing < 1.0$ mm. Before the reaction, catalysts were activated at 723 K under a helium flow (70 cm^3 min^{-1}) for 4 h. The analyses of NO and the reaction products were made with gas chromatography using a 13X molecular sieve + Porapak Q column working at 333 K. In the experiments with sulfur poisoning, after 1 h, the reaction of the NO decomposition was stopped and for 30 min SO_2 was passed through the catalyst bed at the reaction temperature; after that the decomposition of NO was resumed.

RESULTS

H_2 TPR

The H_2 TPR profiles of Cu-containing materials are shown in Figs. 1–3. Two peaks in the TPR profile of Cu–NbZSM-5-52 (52% Cu exchanged) (Fig. 1) originate from Cu^{2+} reduction in two steps (to Cu^+ and to Cu^0). According to the literature (29) concerning Cu–AlZSM-5 zeolites, with the increasing Cu exchange level the difference in the reduction temperature of the first step ($Cu^{2+} \rightarrow Cu^+$) and the second step ($Cu^+ \rightarrow Cu^0$) decreases, which results in the connection of two TPR peaks into one broader peak. It is true also for Nb-containing zeolites, as documented in Fig. 1 (compare the results for Cu–NbZSM-5-52 and Cu–NbZSM-5-106). A small shoulder at ∼473 K can be assigned to the reduction of CuO species, as shown in Fig. 2a (CuO reduction profile).

Cu–AlZSM-5-120 (120% exchanged) exhibits one broad peak with the maximum at 646 K, i.e., at a much higher

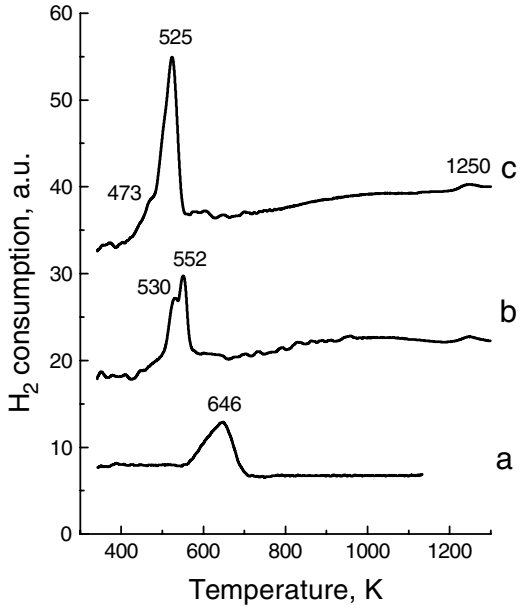

FIG. 1. The effect of the Cu-exchange level in NbZSM-5 and the comparison between Cu–AlZSM-5 and Cu–NbZSM-5. H_2 TPR profiles of Cu–AlZSM-5-120 (a), Cu–NbZSM-5-52 (b), and Cu–NbZSM-5-106 (c).

temperature for this compound than for Cu–NbZSM-5-106. A small peak at 1250 K is due to the reduction of Nb located in the framework, as was the case for NbMCM-41 (30, 31, 34).

The temperature of the H_2 TPR peak maximum is higher for Cu–NbZSM-5-52 than for Cu–NbZSM-5-106, showing that the reducibility of copper cations in NbZSM-5 zeolites by hydrogen increases with Cu loading.

The reducibility of copper cations by hydrogen is easier in ZSM-5-type zeolites when niobium instead of aluminum is incorporated into the lattice. This means that the interaction of copper with the reductant in the NbZSM-5 matrix is stronger than that in AlZSM-5.

The reduction peak of CuO is registered at 487 K (Fig. 2a). In the TPR profiles of both mixtures (CuO + NbZSM-5 and CuO + AlZSM-5) there are only shoulders at the temperature assigned to CuO reduction. Please note that the mixtures were activated before TPR experiments at 723 K under helium flow. Most probably the solid-state Cu exchange partially occurred under these conditions, which results in H_2 TPR peaks similar to those obtained for the cation-exchanged materials presented in Fig. 1. The difference between Figs. 1 and 2 is in the maximum temperature, which shifted in Fig. 2 toward lower values in the case of the aluminum-containing sample and to higher temperatures in the niobium-containing one.

The additional peaks (555 and 575 K) which appear after sulfation of Cu–NbZSM-5-106 (Fig. 3b) are due to the reduction of copper sulfate species. It is noteworthy that the temperatures of maxima in the TPR profile of sulfated Cu–NbZSM-5 are lower than those noted for $CuSO_4$ (600 and 680 K) and Cu–AlZSM-5, as reported in our earlier paper (27). In Fig. 3b two shoulders in the range 600–700 K can be due to $CuSO_4$ formed with the participation of overexchanged copper. That leads to the conclusion that copper sulfate species in a Nb-containing matrix are less stable than those in AlZSM-5. The negative charge of the NbZSM-5 lattice makes the reduction of copper sulfate

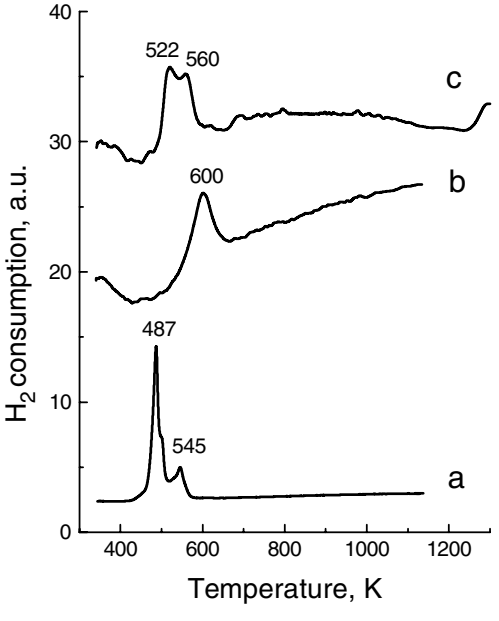

FIG. 2. H_2 TPR profiles of CuO (a), CuO + AlZSM-5 (b), and CuO + NbZSM-5 (c).

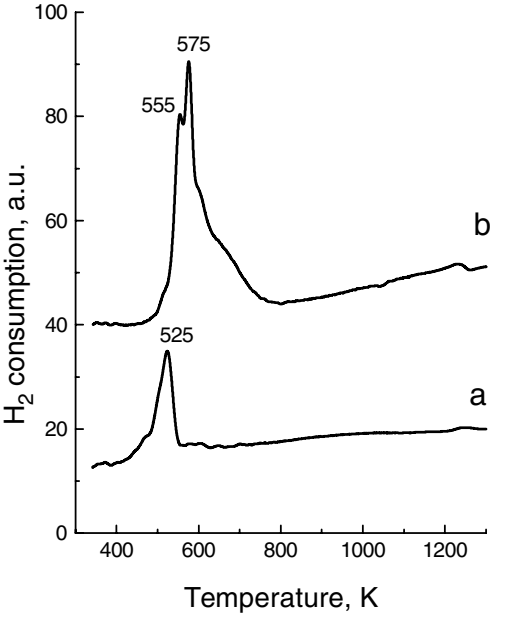

FIG. 3. The effect of sulfation on H_2 TPR profiles: (a) Cu–NbZSM-5-106 and (b) Cu–NbZSM-5-106 after sulfation ($SO_2 + O_2$, heating at 673 K).

species easier in that case than in the case of their location on AlZSM-5.

ESR Study

The interaction of copper species with various zeolite matrices can result in the autoreduction of copper, which occurs during activation under vacuum or under the flow of an inert gas. The reduction levels of Cu^{2+} can be approximately estimated on the basis of the decrease in the intensity of the ESR signal due to Cu^{2+} paramagnetic species. Comparison of the ESR signal-intensity drops caused by the increase in the evacuation temperature of Cu–AlZSM-5-96 versus the signal intensity drops of Cu–NbZSM-5-106, exhibited in Fig. 4, indicates that autoreduction of Cu^{2+} occurs a little more easily on an aluminosilica than on a niobiosilica matrix. If one compares the intensity of the ESR signal after evacuation at 723 K on both samples the following values are obtained: Cu–AlZSM-5-96, 90% reduction; Cu–NbZSM-5-106, 77% reduction. The difference is more visible after evacuation at lower temperatures, for example at 473 K: Cu–AlZSM-5-96, 68% reduction; Cu–NbZSM-5-106, 47% reduction. However, the decrease in the Cu^{2+} ESR signal intensity due to evacuation up to 473 K is not caused by the reduction in copper cations. According to (35, 36) the early stages of dehydration (from room temperature to about 470 K) involve cupric ion migration and formation of ESR-silent moieties but not reduction to Cu^{+}.

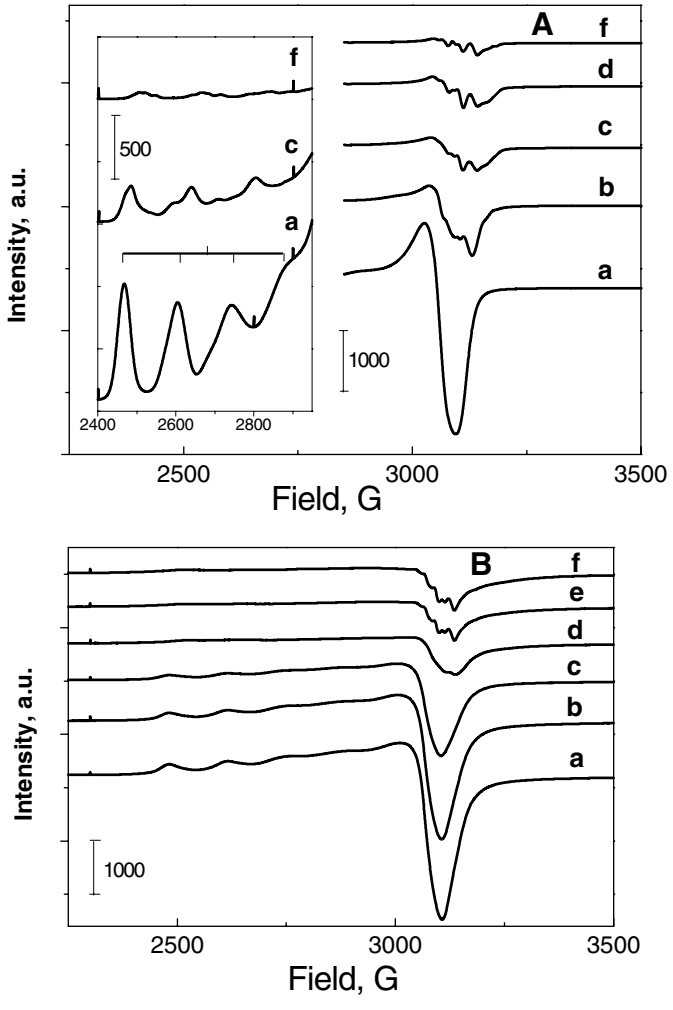

FIG. 4. ESR spectra of Cu-containing NbZSM-5 and AlZSM-5 zeolites evacuated at various temperatures (spectra recorded at 77 K). Cu–AlZSM-5-96 (A) and Cu–NbZSM-5-106 (B); the samples were evacuated at RT (a), 373 K (b), 473 K (c), 573 K (d), 673 K (e), and 723 K (f).

TABLE 2

ESR Parameters Determined for the Different Catalysts

Catalyst	Treatment	Octahedral		Square pyramidal		Square planar	
		$g_\parallel$	$A_\parallel$	$g_\parallel$	$A_\parallel$	$g_\parallel$	$A_\parallel$
Cu–AlZSM-5-96	Fresh	2.38	137				
	Evac. RT	2.38	137				
	Evac. 373 K			2.34	156		
	Evac. 473 K			2.32	143	2.28	168
	Evac. 723 K			2.32	143	2.27	169
	Ads. NO			2.32	144	2.28	169
Cu–NbZSM-5-106	Fresh	2.37	135				
	Evac. RT	2.37	135				
	Evac. 373 K	2.37	136				
	Evac. 473 K	2.37	133				
	Evac. 573 K			2.34	134		
	Evac. 673 K			2.34	131		
	Evac. 723 K			2.34	140	2.28	162
	Ads. NO			2.34	148		

Note. $A_\parallel$ is given in gauss.

A difference between studied samples is also manifested in the coordination of copper after the same temperature treatment. This is shown in Table 2, summarizing the g factors. The transformation of Cu-octahedral into Cu-square pyramidal structures on Cu–AlZSM-5 occurs at 373 K (during the evacuation), whereas on Cu–NbZSM-5 it takes place at 573 K. The next transformation to a square planar structure is only slightly observed on Cu–NbZSM-5 after evacuation at 723 K and is very visible on Cu–AlZSM-5 evacuated at 473 K. A values (Table 2) are lower when the Nb-containing matrix is applied. It is worth noting that the considered changes in Cu coordination correspond only to residual ESR-visible Cu^{2+} cations. One cannot exclude the possibility that a part of the ESR-silent Cu^{2+} moieties transform also to square planar structures and cannot be registered.

The autoreduction of copper and the removal of ligands leading to the coordination changes are more difficult on Cu–NbZSM-5 than on Cu–AlZSM-5 samples. This seems to be in agreement with the easier reduction of copper by hydrogen on the Nb-containing matrix (H_2-TPR results), because it indicates stronger interaction of Cu with

ligands, i.e., stronger reaction with the reagent (hydrogen or SO_2). If the model of the NbMCM-41 framework (30, 31, 34) were adapted to NbZSM-5, one can state that in Cu–NbZSM-5 there would be a lower number of OH groups in the surrounding copper species and therefore autoreduction in it of copper would be more difficult than in Cu–AlZSM-5.

NO adsorption on Cu–AlZSM-5 evacuated at 723 K leads to the formation of a Cu^+NO complex and to the oxidation of copper to Cu^{2+} (the increase in the ESR signal intensity—Fig. 5A, spectrum b). This means that the material evacuated at 723 K has Cu^+ ions and that copper-reduced species are easily oxidized by NO.

The effect of NO adsorption on Cu–NbZSM-5 (Fig. 5B) is the same concerning copper oxidation. The ESR signal (Fig. 5B, spectrum d) formed is not typical for Cu^+NO but can be assigned to the $Cu^{2+}O^-NO$ paramagnetic complex (32) or to the other $Cu^{\delta+}NO$ species. Comparison of spectra a and c (Fig. 5B) indicates that NO adsorption is a reversible process.

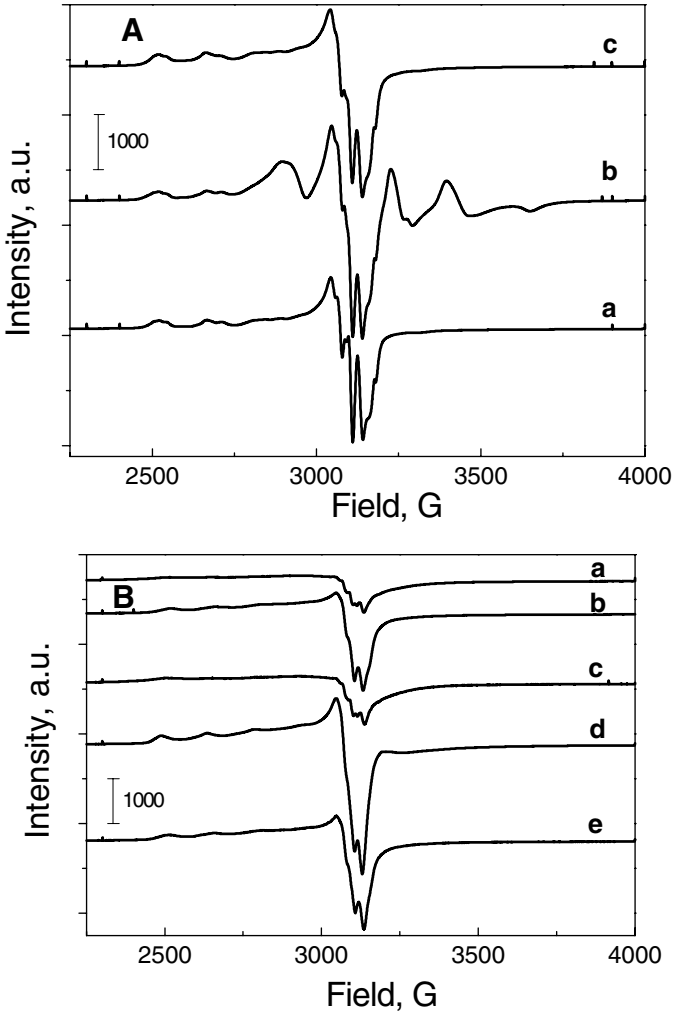

FIG. 5. The effect of NO adsorption—ESR spectra recorded at 77 K. (A) Cu–AlZSM-5-96 (a) evacuated at 723 K, (b) after NO adsorption at RT, and (c) followed by evacuation at 473 K. (B) Cu–NbZSM-5-106 (a) after evacuation at 723 K, (b) after NO adsorption at RT and evacuation at RT, (c) followed by evacuation at 723 K, (d) after next adsorption of NO, and (e) after evacuation at RT.

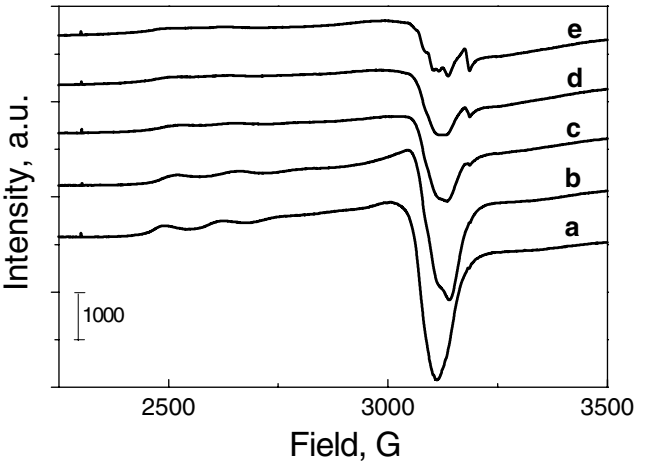

FIG. 6. CuO transformation on the zeolite matrix—ESR spectra recorded at 77 K. CuO + NbZSM-5: fresh sample (a) and after evacuation at 373 K (b), 473 K (c), 573 K (d), and 673 K (e).

When the mixture of CuO + NbZSM-5 is evacuated at increasing temperatures the ESR spectra show, first, the paramagnetic Cu^{2+} species, but from 473 K an additional ESR signal appears (Fig. 6). Its intensity increases with the activation temperature and its g value (2.005) is close to that for oxygen radicals connected with Nb. H_2-TPR results (Fig. 2) also indicated the decomposition of CuO. Very probably the increase in the temperature leads to the decomposition of CuO and oxygen is trapped on Nb sites, forming radical species.

FTIR Study

Infrared spectroscopy allows differentiation between copper and niobium active species which interact with NO molecules. We focus on the study of the spectral range characteristic of NO adsorption on transition metals (33).

When NO is adsorbed on the dehydrated NbZSM-5 zeolites two main broad IR bands, at 1896 and 1602 cm^{-1}, are recorded (Fig. 7A). It was stated earlier (28) that there is Nb(V) in the zeolite structure. Therefore, one can suppose that the dehydroxylation of NbZSM-5 can occur according to Scheme 1, proposed for NbMCM-41 molecular sieves (31, 34). The IR band at 1602 cm^{-1} can be assigned to NO adsorbed on NbO^- skeletal species and its wavenumber is lower than that for the same complex detected in NbMCM-41 (1630 cm^{-1}), suggesting a weaker N–O bond after adsorption on NbZSM-5. The nitrosyl species ($\nu(NO)^{\delta-}$) reported in many papers can be observed in the

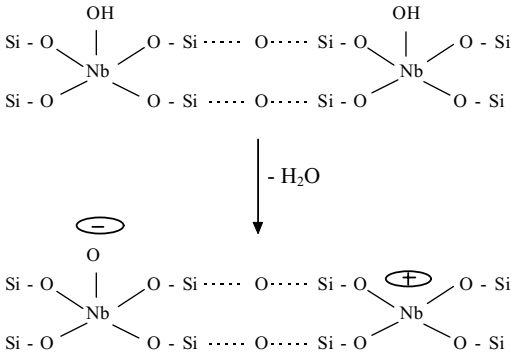

SCHEME 1

region 1800–1819 cm^{-1} (37, 38). In the spectra of Fig. 7 in this region a small shoulder is detectable. A broad band at 1896 cm^{-1} could be related to N_2O_3 species (5, 37) formed as a result of dinitrosil coordinated with the oxygen from the lattice of the catalyst. The evacuation at RT (Fig. 7A, spectrum c) causes decrease in the 1896-cm^{-1} band and growth of that at 1602 cm^{-1}, showing the migration and decomposition of N_xO_y species under the dynamic conditions (evacuation).

The Cu ion exchange in NbZSM-5 leads to important changes in the IR spectra (Figs. 7B and 7C), strongly enhancing adsorbed species intensity. For the sample with a higher Cu-exchange level (Fig. 7B) three IR bands are observed: at 1886 cm^{-1} (the most intense), due to the $Cu^{2+}NO$ complex (17, 39), and at 1783 and 1604 cm^{-1}. The latter cannot originate from NbO^-NO species as in NbZSM-5 because it is not visible when a lower Cu-exchange degree is applied (Fig. 7C). Therefore, we assigned this band to the $Cu^{2+}(O^-NO)(NO)$ complex (37, 38) ($Cu^{2+}O^-$ formed during the autoreduction of copper). The NbO^-NO complex is not formed because Cu cations cover NbO^- species. The origin of a band at 1783 cm^{-1} is not clear. This band could be tentatively assigned to the $Cu^{\delta+}NO$ species ($\delta < 1$) because when the sample is oxidized before NO adsorption, the intensity of this feature is very low (Fig. 8A). Moreover, the intensity is lowered when the Cu-exchange level is lower (comparison of Figs. 7B and 7C). It is known that the reduction in Cu increases with the cation-exchange degree. The negative charge located on nonbridged Nb-O^- in the skeleton of the zeolite makes the copper reduction deeper than in the case of the AlZSM-5 matrix. The reduced copper is less bonded to oxygen (NbO^-) and therefore more metallic (niobium exhibits a greater cationic character). When NO is adsorbed on the surface a back-donation effect takes place (electrons go from $Cu^{\delta+}$ to NO molecule) and the position of the $\nu(NO)^{\delta-}$ IR band shifts to lower wavenumbers.

Figure 8 compares the effect of NO adsorption on Cu–NbZSM-5-106 and Cu–AlZSM-5-120, which were oxidized before the NO adsorption. The latter shows the following bands: 1638 cm^{-1}, due to water (confirmed by the broad band in the OH region, not shown here); 1734 cm^{-1}, from $Cu^+(NO)_2$ (5, 9, 13, 37); 1811 cm^{-1}, due to Cu^+NO complex (5, 9, 13, 37); 1896 cm^{-1}, with a shoulder at ~1880 cm^{-1} that covers two $Cu^{2+}NO$ species (17, 40, 41); 2129 cm^{-1} (NO^+)

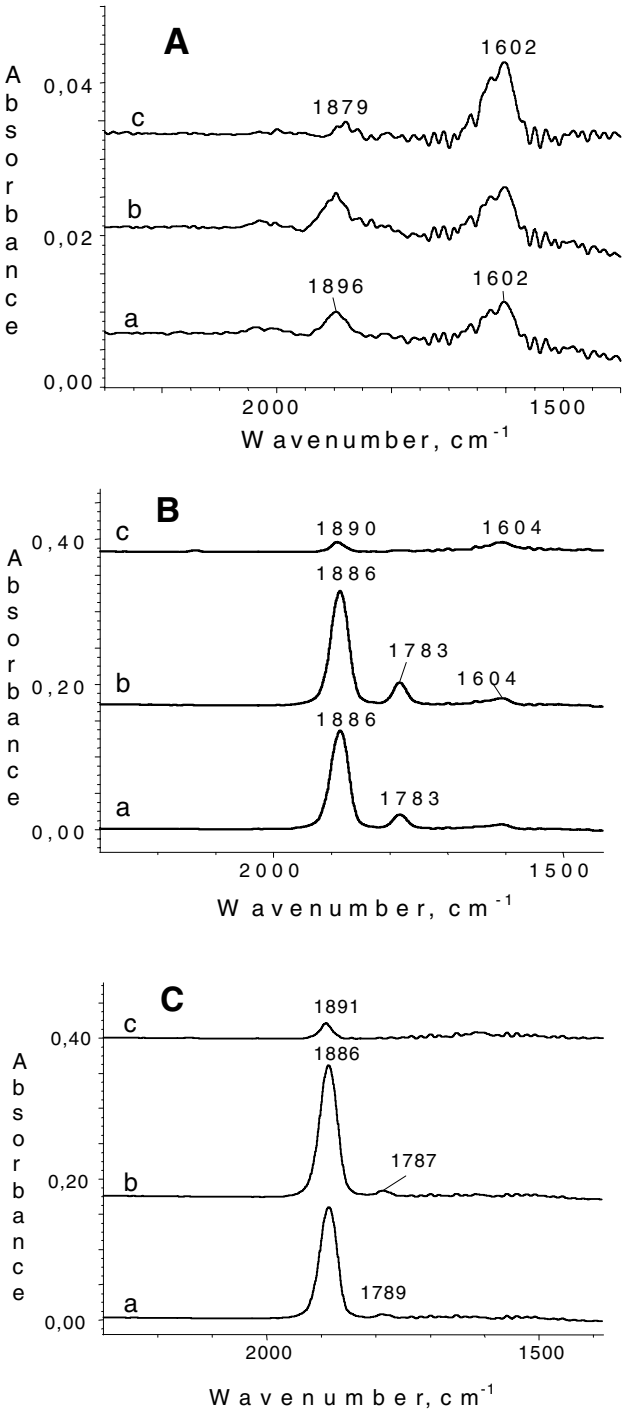

FIG. 7. FTIR subtracted spectra of NbZSM-5 after the following operations. (A) NbZSM-5: NO adsorption at RT of (a) 0.4 mmol g^{-1} and (b) full saturated sample; (c) evacuation at RT, 15 min. (B) Cu–NbZSM-5-106: NO adsorption at RT of (a) 0.2 mmol g^{-1} and (b) 0.4 mmol g^{-1}; (c) evacuation at RT, 15 min. (C) Cu–NbZSM-52: NO adsorption at RT of (a) 0.4 mmol g^{-1} and (b) full saturated sample; (c) evacuation at RT, 15 min.

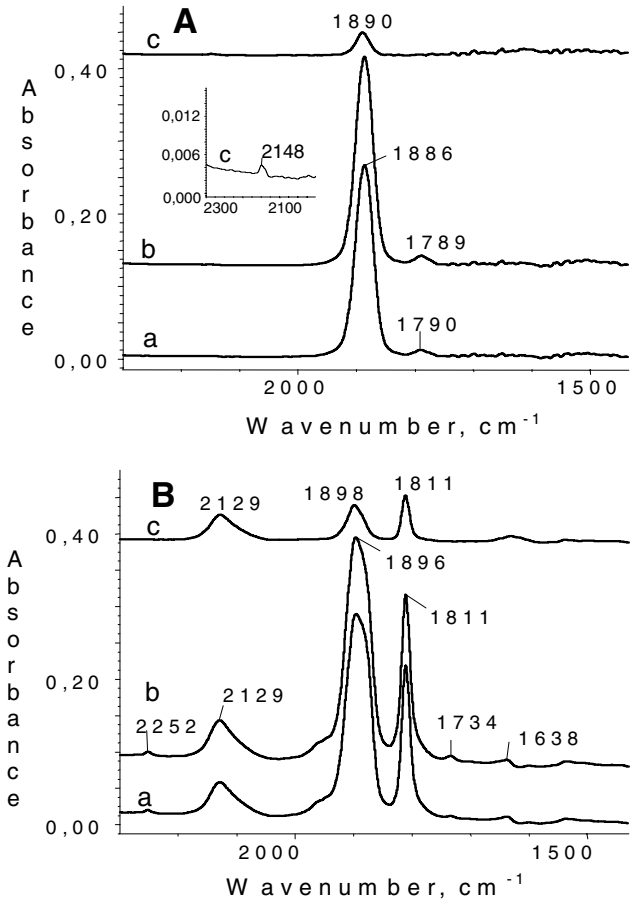

FIG. 8. FTIR subtracted spectra of ZSM-5 oxidized before NO adsorption and after the following operations. (A) Cu–NbZSM-5-106: NO adsorption at RT of (a) 0.4 mmol g^{-1} and (b) full saturated sample; (c) evacuation at RT, 15 min. (B) Cu–AlZSM-5-120: NO adsorption at RT of (a) 0.4 mmol g^{-1} and (b) full saturated sample; (c) evacuation at RT, 15 min.

(13, 42); and 2252 cm^{-1} (N_2O) (5, 37). The formation of NO^+ is accompanied by the appearance of H_2O according to the following reaction scheme proposed by Hadjiivanov *et al.* (42):

$$2NO + 1/2O_2 + 2O_{lattice} - H^+ \rightleftarrows H_2O + 2O_{lattice} - NO^+.$$

Calculation of the absorbance ratios $Cu^+NO/Cu^{2+}NO$ for Cu–AlZSM-5-120 and $Cu^{\delta+}NO/Cu^{2+}NO$ for Cu–NbZSM-5-106 shows the values ~0.7 and 0.1, respectively. It clearly indicates that the number of reduced Cu species is higher in Cu–AlZSM-5 zeolite than in the Nb-containing sample. NO^+ is formed very easily on Cu–AlZSM-5-120 whereas it is only slightly visible on Cu–NbZSM-5-106 when an excess of NO is evacuated (Fig. 8A, spectrum c). However, NO^+ cations are registered when a Cu–Nb-containing zeolite is heated in the presence of adsorbed NO (Fig. 9B).

The formation of NO^+ is less pronounced when the Cu-exchange level is lower (Cu–NbZSM-5-52). Moreover, it is not detected when the Nb-containing samples are oxidized prior to NO adsorption and when a CuO + NbZSM-5 mixture is used. In the latter case the activation of the mixture leads to the solid-state cation exchange, as suggested by the above-described experiments (H_2-TPR, ESR). One can conclude that the autoreduction of copper in the cation-exchanged material causes the formation of OH groups, which are necessary for the production of NO^+ (42). The absence of OH groups in the cation solid-state-exchanged zeolites is a reason for NO^+ absence even after heating to 673 K.

NO^+ is generated at RT on Cu–AlZSM-5-120 (Fig. 9A) as a result of the interaction of NO with hydroxyls (43). Water, which is formed in this reaction, is chemisorbed on the surface. Increasing temperatures leads to a decrease in NO^+ band intensity and to the appearance of a band at about 1533 cm^{-1}, most probably due to N_2O_3 (5, 37, 43). At a higher temperature the mobility

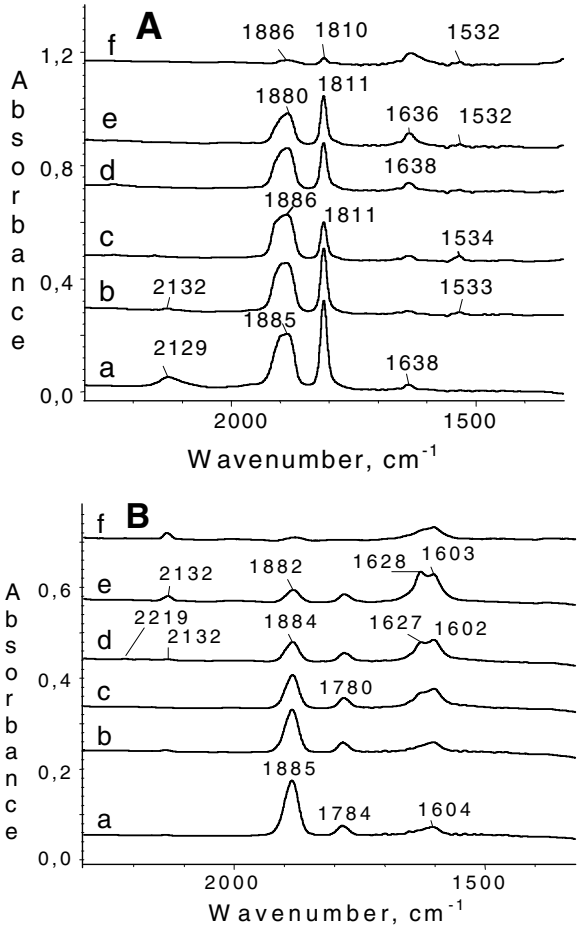

FIG. 9. FTIR spectra of (A) Cu–AlZSM-5-120 and (B) Cu–NbZSM-5-106 after the following operations: (a) NO adsorption at RT (0.4 mmol/g); (b) heating at 373 K, (c) 473 K, (d) 573 K, and (e) 673 K; and (f) evacuation at RT, 15 min.

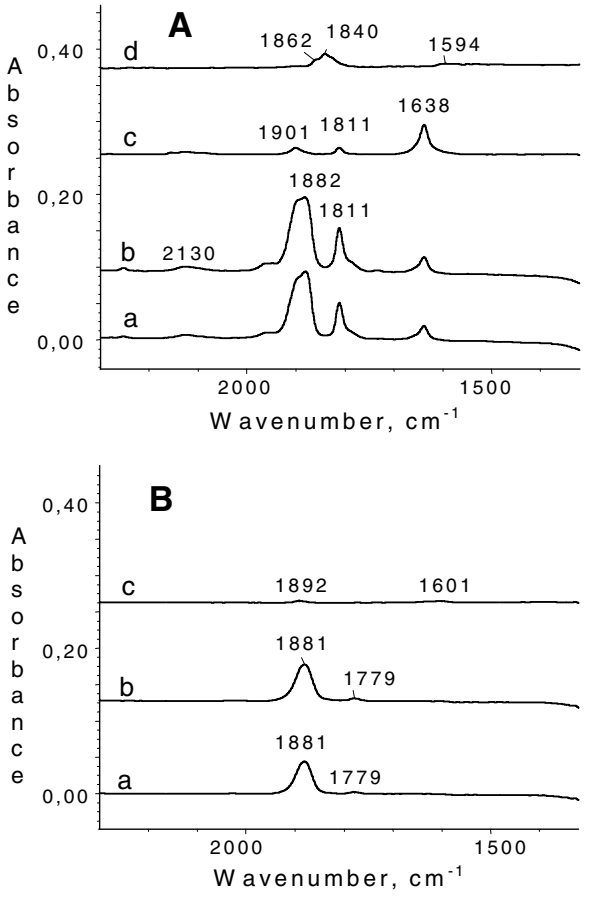

FIG. 10. FTIR subtracted spectra of CuO + ZSM-5 after the following operations. (A) CuO + AlZSM-5: NO adsorption at RT of (a) 0.4 mmol g^{-1} and (b) full saturated sample; (c) evacuation at RT, 15 min; and (d) CuO after NO adsorption (0.4 mmol g^{-1}). (B) CuO + NbZSM-5: NO adsorption at RT of (a) 0.4 mmol g^{-1} and (b) full saturated sample; (c) evacuation at RT, 15 min.

of chemisorbed water increases and therefore it interacts with NO^+, forming N_2O_3 and regenerating the acidic OH groups.

The NO-adsorbed species that are formed on activated CuO + ZSM-5 (both Nb and Al) are like those noted for Cu-cation exchanged materials, but the relative intensity of the IR bands varies (Fig. 10). The spectra of NO adsorbed on CuO (Fig. 10A, spectrum d) display IR bands different from those found when NO is adsorbed on copper existing in AlZSM-5 or NbZSM-5. These results confirm the solid-state ion exchange during activation of a mixture of CuO + ZSM-5 suggested on the basis of H_2-TPR and ESR studies.

The effect of SO_2 adsorption on NO chemisorption and transformation on Cu–NbZSM-5-106 is illustrated in Fig. 11. After SO_2 adsorption at RT weakly coordinated SO_2 is registered at 1338 cm^{-1}. A small shoulder at a higher wavenumber can be due to the SO_2 chemisorbed species. It is visible that adsorbed sulfur dioxide does not block all the species responsible for the adsorption of NO, because the intensities of IR bands due to $Cu^{2+}NO$ and $Cu^{\delta+}NO$ (Fig. 11A, spectrum a) are the same as those noted without SO_2 preadsorption (Fig. 7B, spectrum a). However, after preadsorption of SO_2 the complex $Cu^{2+}(O^-NO)$ (NO) (1604 cm^{-1}) is not registered. Moreover, heating at 573 K (Fig. 11A, spectrum b) causes a decrease in the intensity of a band at 1886 cm^{-1} ($Cu^{2+}NO$), indicating a replacement of such adsorbed NO by chemisorption of SO_2 (a shoulder at ~1360 cm^{-1} is more visible in spectrum b). The evacuation at RT removes physisorbed SO_2, with sulfur dioxide (1364 cm^{-1}) remaining chemisorbed. The latter blocks Cu^{2+} sites for NO adsorption, as documented in Fig. 11A, spectrum c. Evacuation at 723 K (spectrum d) leads to the removal of all NO adsorbed species and leaves SO_2 chemisorbed. This chemisorbed sulfur dioxide gives the same features as in Fig. 11B, formed by $SO_2 + O_2$ treatment

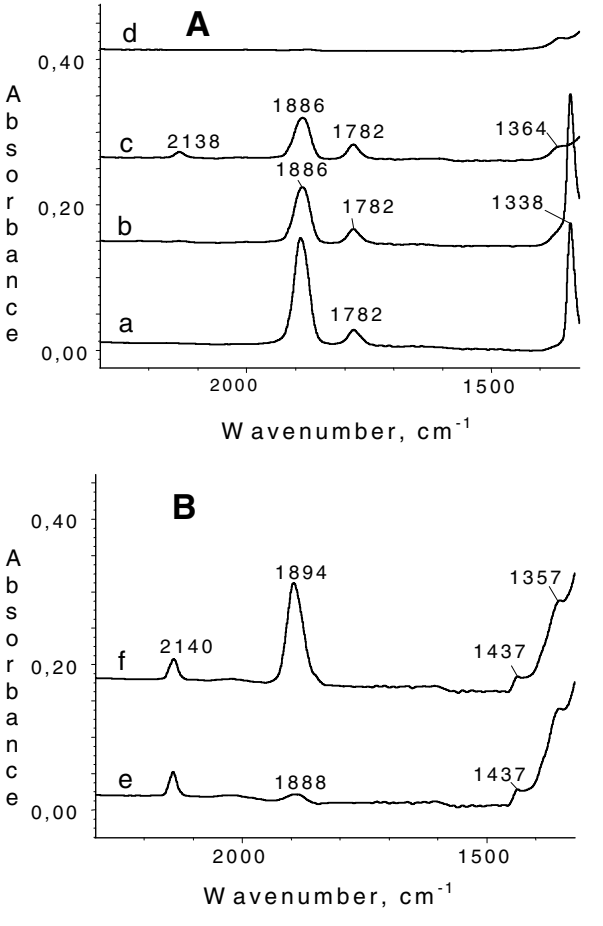

FIG. 11. FTIR subtracted spectra of Cu–NbZSM-5-106 after the following operations. A: (a) NO adsorption at RT (0.2 mmol g^{-1}) after SO_2 preadsorption at RT (0.3 mmol g^{-1}) followed by evacuation at RT, 15 min; (b) heating at 573 K; (c) NO adsorption at RT (0.2 mmol g^{-1}) followed by evacuation at RT, 15 min; (d) evacuation at 723 K, 15 min. B: (e) Adsorption of SO_2 (0.3 mmol g^{-1}) + O_2, heating at 673 K, 30 min, evacuation at RT, 15 min; and (f) NO adsorption (0.2 mmol g^{-1}) at RT.

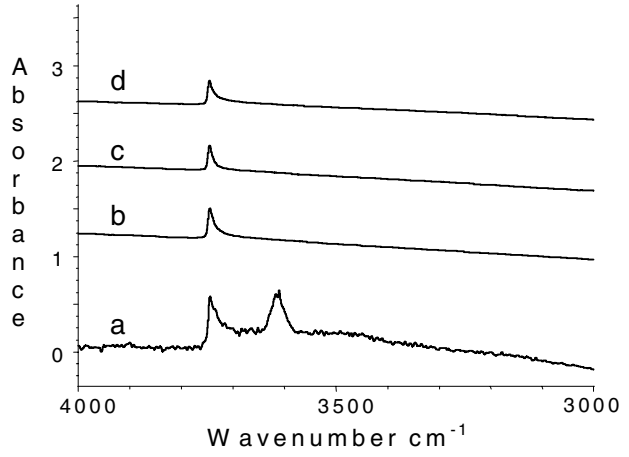

FIG. 12. ν(OH) stretching region of Cu–AlZSM-5-120 (a), Cu–NbZSM-5-52 (b), Cu–NbZSM-5-106 (c), and NbZSM-5 (d) samples after activation.

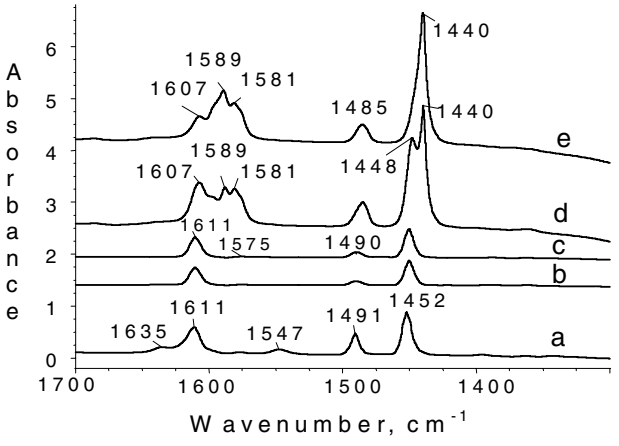

FIG. 13. Pyridine adsorption after activation, then desorption at 423 K on Cu–AlZSM-5-120 (a), Cu–NbZSM-5-52 (b), and Cu–NbZSM-5-106 (c); pyridine adsorption after activation without evacuation on Cu–NbZSM-5-106 (d) and NbZSM-5 (e).

at 673 K (a shoulder at 1357 cm^{-1}—Fig. 11B, spectrum a), so it can be interpreted as a sulfate species. The other sulfate species described by an IR band at 1437 cm^{-1} blocks $Cu^{\delta+}$ sites, because after NO adsorption a band at ~1780 cm^{-1} is not registered (spectrum f). According to the literature (27, 44, 45) the IR band at 1437 cm^{-1} can be assigned to sulfate species of type II.

Acidity Measurements

Figure 12 shows IR spectra of the activated Cu–AlZSM-5-120 (Fig. 12a), Cu–NbZSM-5-52 (Fig. 12b), Cu–NbZSM-5-106 (Fig. 12c), and Nb-ZSM-5 (Fig. 12d) samples in the ν(OH) stretching region. We observe that for Cu–AlZSM-5-120 two bands are present, at 3745 and 3610 cm^{-1}, assigned to terminal SiOH and bridged Si(OH)Al hydroxyls, respectively. In contrast, on niobium-substituted zeolites only the band due to silanols is detected.

Acidity measurements have been performed by pyridine adsorption on the activated samples, then evacuation at increasing temperatures.

The sample Cu–AlZSM-5-120 (Fig. 13a) presents both Brønsted (1635 cm^{-1}) and Lewis sites of mild acid strength (1611 cm^{-1}), typical of pyridine coordinated with Cu^{+}. The probes remain bonded to the surface up to 723 K under dynamic evacuation, showing strong coordination acid sites.

In the presence of niobium, as shown in the spectra of samples Cu–NbZSM-5-52 and Cu–NbZSM-5-106 (Figs. 13b and 13c) Brønsted acidity is inhibited by niobium addition (in agreement with the absence of OH acid groups), while Lewis acidity remains almost unchanged. The probe molecule coordination versus temperature seems weaker, since the intensity of the adsorption features strongly decreases already after desorption at 523 K. Interestingly after pyridine adsorption at RT, the spectrum of Cu–NbZSM-5-106 (Fig. 13d) shows a split ν_{19b} stretching mode, with a doublet, at 1448 and 1440 cm^{-1}. The same was recorded on Cu–NbZSM-5-52 (not shown in Fig. 13). The first peak belongs to pyridine coordinated with Cu^{+} and the second could be related to the presence of Nb cations. To confirm this hypothesis we adsorbed pyridine on a NbZSM-5 sample (without copper), as reported in Fig. 13, spectrum e; a sharp band appears at 1440 cm^{-1}. This frequency is very close to that of liquid pyridine (46) (1436 cm^{-1}), meaning that a very weak interaction takes place between the probe and the surface site. Probably it is just because of this weak bond that a difference between copper and niobium cations can be detected, whereas strong pyridine chemisorption gives rise to unresolved features for other elements. Similar results were found with CO weak adsorption on oxides (47).

Activity in NO Decomposition

The activity of Cu-containing ZSM-5 zeolites in the NO decomposition at various temperatures expressed by turnover frequency (TOF) numbers is shown in Table 3 and NO conversion versus temperature is plotted in Fig. 14. Cu located in a NbZSM-5 matrix (52% Cu) gives rise to TOF

TABLE 3

TOF (Number of NO Molecules Converted per Cu Ion per Second $\times 10^{-3}$) of the Catalysts in the Decomposition of NO

Catalyst	573 K	623 K	673 K	723 K	773 K	823 K	923 K	973 K
Cu–AlZSM-5-120	0.7	1.3	1.5	3.6	4.2	3.7	2.9	1.4
Cu–NbZSM-5-52	2.1	2.9	3.4	3.1	2.3	1.6	1.0	0.5
Cu–NbZSM-5-106	1.2	1.5	2.4	2.0	1.7	1.5	1.2	0.9

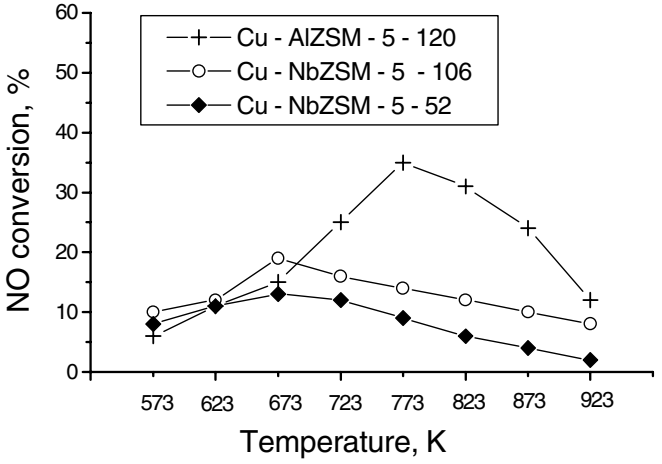

FIG. 14. NO conversion on ZSM-5 zeolites. Influence of reaction temperature.

numbers a little lower than those in the case of AlZSM-5 zeolite used above 673 K. But it is much more active at lower temperatures. The higher loading of NbZSM-5 with Cu (106%) causes a lower TOF. The maximum activity (3.4×10^{-3} TOF) of Cu–NbZSM-5-52 is reached at 673 K whereas that for Cu–AlZSM-5-120 (4.2×10^{-3} TOF) is at 773 K. The NO conversion, shown in Fig. 14, is almost the same for all samples at low temperatures (573–673 K) and significantly differs at higher temperatures. Above 673 K Cu–AlZSM-5 exhibits higher NO conversion than both Nb-containing materials, which are deactivated at these temperatures. SO_2 adsorption at the reaction temperatures leads to a decrease in the NO conversion in both Cu–AlZSM-5-120 and Cu–NbZSM-5-106. This effect for the latter sample is illustrated in Fig. 15 and that for Cu–AlZSM-5-120 is shown in (27).

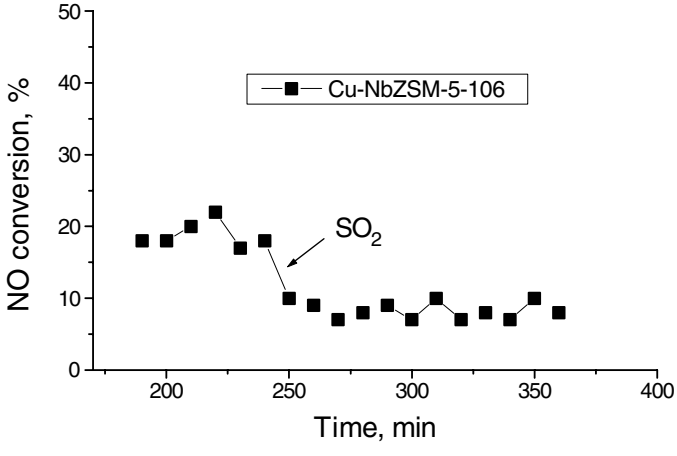

FIG. 15. NO conversion at 673 K on Cu–NbZSM-5-106 before and after poisoning with SO_2 (the arrow indicates a time when the reaction started after SO_2 poisoning).

DISCUSSION

The incorporation of niobium instead of aluminium into the MFI structure changes the physicochemical properties of the obtained molecular sieve. The results presented in this paper indicating the location of copper in the extra framework cation position show that NbZSM-5 zeolite has extra framework cations or protons easily exchangeable for copper cations in an aqueous solution of a copper salt. Copper cations in Cu–NbZSM-5 were registered in ESR spectroscopy and FTIR spectra after NO adsorption. One should consider the possibility of impregnation during NbZSM-5 treatment using a solution of copper acetate. It can lead to the formation of a CuO phase after calcination. However, the observed infrared bands cannot be due to NO adsorbed on CuO because, as Fig. 10 documently nitrogen oxide chemisorbed on pure CuO gives rise to a different position of IR bands. Moreover, X-ray diffusion studies did not show features due to the CuO crystal phase. H_2-TPR profiles of Cu–NbZSM-5-106 and Cu–NbZSM-5-52 exhibit only a small shoulder at ~473 K due to the reduction of CuO (Fig. 1) and very intensive signals assigned to the two reduction steps: $Cu^{2+} \rightarrow Cu^{+} \rightarrow Cu^{0}$.

It is noteworthy that the material prepared by mixing CuO with NbZSM-5 and activated at the conditions used before H_2-TPR and FTIR experiments did not show CuO phase. Both H_2-TPR profiles (Fig. 2) and FTIR spectra (Fig. 10) indicate the presence of copper cations located in the extraframework position. This allows the statement that solid-state cation exchange occurred in the mixture of CuO and NbZSM-5.

All these results brought us to a conclusion about the location of Nb in the skeleton of the zeolite and the presence of a negative charge in the framework being responsible for cation-exchange properties. In the first paper concerning NbZSM-5 zeolites (28) (denoted NbS-1) ESR studies provided evidence for the incorporation of Nb(V) into the silica framework. However, the possibility of a small amount of extraframework Nb_2O_5 cannot be excluded. The results presented in this paper confirm this statement and allow us to adapt the dehydroxylation scheme proposed for NbMCM-41 (34) for NbZSM-5 material. Moreover, infrared spectra of the ν(OH) stretching region (Fig. 12) show that no bridged OH groups are present in the Nb-containing material (in fact no pyridinium ion formation is shown after pyridine adsorption), supporting the statement that niobium incorporation occurs. In the parent NbZSM-5 material NbOH (or Na) nonbridged species are present. Protons or Na cations are exchanged for hydrated copper. Copper hexa aqueous complexes decompose during calcination and form a small number of nonbridged OH groups, which are less acidic than those formed in Cu–AlZSM-5. The presence of acidic OH groups in Cu–AlZSM-5 is evidenced also from FTIR studies (Figs. 8 and 9) showing the formation

of NO^+ after nitrogen oxide adsorption. However, NO^+ cations (IR band at ~2130 cm^{-1} (42)) are formed more easily on Cu–AlZSM-5 (Fig. 8B) than on Cu–NbZSM-5 (Fig. 9B). The latter is able to generate NO^+ species at higher temperatures, confirming the lower acidity of OH groups in the zeolite lattice containing niobium. The lower acidity of OH groups in Cu-NbZSM-5 is clear, taking into account the location of the acidic proton in the nonbridged position connected with NbO^- species. The proton is held more strongly by NbO^- than in the bridged position (Al–OH–Si) in aluminosilica ZSM-5 zeolite. Moreover, the concentration of OH groups located in the surroundings of NO chemisorbed on copper species is lower in Cu–NbZSM-5 than in Cu–AlZSM-5. This is one reason for the more difficult interaction between OH groups and chemisorbed NO, leading to the formation of NO^+ (42). The mobility of protons in Cu–NbZSM-5 increases with temperature and allows the interaction with NO.

The autoreduction of copper in the MFI matrix during evacuation or activation in the flow of an inert gas strongly depends on the nature of the *T* element in the framework. A slightly lower number of Cu^{2+} cations is reduced under the same conditions on Cu–NbZSM-5 than on Cu–AlZSM-5, as shown from the ESR results (Fig. 4). However, the reduction of copper in the Nb-containing matrix is deeper than that in the aluminosilica zeolite. There is no ESR signal due to the Cu^+NO complex, as on Cu–AlZSM-5 zeolite, and the IR band originating from Cu^+NO (1811 cm^{-1}) is shifted to a lower wavenumber on Cu–NbZSM-5 (1783 cm^{-1}), indicating that copper is more metallic than Cu^+; i.e., it is $Cu^{\delta+}$ ($\delta < 1$). Moreover, Cu^{2+}–ligand interaction is stronger in Cu–NbZSM-5 than in Cu–AlZSM-5, which makes transformation from octahedral to square pyramidal and square planar structures more difficult in Nb-containing sieves (Table 2). The tendency to the stronger bonding of ligands may be one reason for the easier reduction of copper by hydrogen (a stronger interaction of copper with hydrogen) observed in H_2-TPR profiles (Figs. 1 and 2). Copper sulfate species are also more easily reduced by hydrogen when Cu^{2+} or $Cu^{\delta+}$ is connected with NbO^- in the zeolite framework (Fig. 3).

Sulfur dioxide preadsorption followed by NO adsorption on Cu–NbZSM-5 zeolite causes the formation of sulfate species at 573 K which block Cu^{2+}, $Cu^{\delta+}$, and $Cu^{2+}O^-$ species (Fig. 11). This behavior is the same as on Cu–AlZSM-5 and varies from that found for Cu–NbMCM-41 (27). This means that the effect of SO_2 interaction not only is due to the presence of Nb in the framework of the molecular sieve, but also depends on the structure of the material. In the more open structure (NbMCM-41) Nb prevents copper species from being poisoned with sulfate, whereas in the NbZSM-5 matrix this effect is less evident. This is one reason for the deactivation of Cu–NbZSM-5 in the NO decomposition after SO_2 adsorption (Fig. 14).

The activity of Cu-containing ZSM-5 zeolites in the decomposition of NO depends on the nature of the *T* element in the framework. The presence of Nb decreases the maximum of the activity (Table 3), but the temperature at which the maximum is reached is lower in Cu–NbZSM-5 zeolites. Moreover, the increase in the Cu exchange level in Cu–NbZSM-5 causes a decrease in TOF, whereas the NO conversion increases. The strong interaction of Cu^{2+} with NbO^- species in the framework lowers its autoreducibility and weakens its interaction with NO, resulting in lower activity in NO decomposition carried out at higher temperatures. This could also be correlated to the disappearance of the Brønsted acid sites in the Nb-containing samples, sites that could have a role in NO reduction. The reported activity data indicate that at lower temperatures the Nb-containing samples are more active than the Al-containing ones.

CONCLUSIONS

Our studies confirmed that Nb can be incorporated into the silica framework, giving rise to substituted ZSM-5 zeolite with particular cation-exchange properties. The dehydroxylation scheme proposed for NbMCM-41 can be adapted to NbZSM-5 material. The presence of niobium in the ZSM-5 skeleton causes stronger interaction with Cu cations than that on aluminosilicate ZSM-5, as evidenced by FTIR and ESR studies. This feature determines the physicochemical and catalytic properties of Cu–NbZSM-5 zeolites.

The location of niobium instead of aluminum in the framework of ZSM-5 eliminates Brønsted-acidic OH groups from the surface of the Cu–NbZSM-5 zeolite, making the interactions between hydrogen and NO molecules to give NO^+ more difficult. Nevertheless, for zeolites with a small amount of copper, Nb-substituted samples present higher activity for NO decomposition at mild temperatures, a property that could be interesting for practical applications.

ACKNOWLEDGMENTS

This work was partially supported by Polish Committee for Scientific Research (KBN) Grant 3TO9A 102 19. I.S. thanks KBN for Grant 3TO9A 152 18. This research at the University of Houston was supported by the Robert A. Welch Foundation, the Environmental Institute of Houston, and the U.S. National Science Fundation.

REFERENCES

1. Iwamoto, M., Furukawa, H., Mine, Y., Uemura, F., Mikuriya, S., and Kagawa, S., *J. Chem. Soc. Chem. Commun.*, 1273 (1986).
2. Iwamoto, M., Yahiro, H., Tanda, K., Mizuno, N., Mine, Y., and Kagawa, S., *J. Phys. Chem.* **95**, 3727 (1991).
3. Liu, D. J., and Robota, H. J., *Catal. Lett.* **21**, 291 (1993).

4. Zhang, Y., Leo, K. M., Sarofim, A. F., Hu, Z., and Flytzani-Stephanopoulos, M., *Catal. Lett*. **31**, 75 (1995).
5. Aylor, A., Larsen, S. C., Reimer, J. A., and Bell, A. T., *J. Catal.* **157**, 592 (1995).
6. Eränen, K., Kumar, N., and Lindfors, L. E., *Appl. Catal. B* **4**, 213 (1994).
7. Curtin, T., Grange, P., and Delmon, B., *Catal. Today* **36**, 57 (1997).
8. Curtin, T., Grange, P., and Delmon, B., *Catal. Today* **35**, 121 (1997).
9. Ganemi, B., Björnbom, E., and Paul, J., *Appl. Catal. B* **17**, 293 (1998).
10. Moretti, G., *Catal. Lett*. **28**, 143 (1994).
11. Moretti, G., Dossi, C., Fusi, A., Recchia, S., and Psaro, R., *Appl. Catal. B* **20**, 67 (1999).
12. Dossi, C., Fusi, A., Recchia, S., Psaro, R., and Moretti, G., *Microporous Mesoporous Mater.* **30**, 165 (1999).
13. Konduru, M. V., and Chuang, S. S. C., *J. Phys. Chem. B* **103**, 5802 (1999).
14. Konduru, M. V., and Chuang, S. S. C., *J. Catal*. **187**, 436 (1999).
15. Szanyi, J., and Paffett, M. T., *J. Catal*. **164**, 232 (1996).
16. Wichterlova, B., Dedecek, J., and Vondrova, A., *J. Phys. Chem*. **99**, 1065 (1995).
17. Wichterlova, B., Dedecek, J., Sobalik, Z., Vondrova, A., and Klier, K., *J. Catal*. **169**, 194 (1997).
18. Dedecek, J., and Wichterlova, B., *J. Phys. Chem. B* **101**, 10233 (1997).
19. Kucherov, A. V., Gerlock, J. L., Jen, H. W., and Shelef, M., *J. Catal.* **152**, 63 (1995).
20. Matyshak, V. A., Il'ichev, A. N., Ukharsky, A. A., and Korchak, V. N., *J. Catal*. **171**, 245 (1997).
21. Iwamoto, M., Yahiro, H., Mizuno, N., Zhang, W. X., Mine, Y., Furukawa, H., and Kagawa, S., *J. Phys. Chem.* **96**, 9360 (1992).
22. Li, Y., and Hall, W. K., *J. Catal*. **129**, 202 (1991).
23. Park, S. K., Kurshev, V., Luan, Z., Lee, C. W., and Kevan, L., *Microporous Mesoporous Mater.* **38**, 255 (2000).
24. Centi, G., and Parathoner, S., *Appl. Catal.* **132**, 179 (1995).
25. Armor, J. N., Ed., *in* "Environmental Catalysis," ACS Symposium Series, Vol. 552, Am. Chem. Soc., Washington, DC, 1994.
26. Petunchi, J. O., and Hall, W. K., *Appl. Catal. B* **3**, 239 (1994).
27. Ziolek, M., Sobczak, I., Nowak, I., Daturi, M., and Lavalley, J. C., *Top. Catal.* **11**, 343 (2000).
28. Prakash, A. M., and Kevan, L., *J. Am. Chem. Soc*. **120** (13), 148 (1998).
29. Torre-Abreu, C., Ribeiro, M. F., Henriques, C., and Delahay, G., *Appl. Catal. B* **12**, 249 (1997).
30. Ziolek, M., Sobczak, I., Nowak, I., Decyk, P., Lewandowska, A., and Kujawa, J., *Microporous Mesoporous Mater.* **35–36**, 195 (2000).
31. Ziolek, M., Nowak, I., Sobczak, I., Lewandowska, A., Decyk, P., and Kujawa, J., *Stud. Surf. Sci. Catal.* **129**, 813 (2000).
32. Larsen, S. C., Aylor, A. W., Bell, A. T., and Reimer, J. A., *J. Phys. Chem*. **98**, 11533 (1994).
33. Parvulescu, V. I., Grange, P., and Delmon, B., *J. Phys. Chem. B* **101**, 6933 (1997).
34. Ziolek, M., Sobczak, I., Lewandowska, A., Nowak, I., Decyk, P., Renn, M., and Jankowska, B., *Catal. Today* **70**, 169 (2001).
35. Lo Jacono, M., Fierro, G., Dragone, R., Feng, X., D'Itri, J., and Hall, W. K., *J. Phys. Chem. B* **101**, 1979 (1997).
36. Palomino, G. T., Fisicaro, P., Bordiga, S., Zecchina, A., Giamello, E., and Lamberti, C., *J. Phys. Chem. B* **104**, 4064 (2000).
37. Cheung, T., Bhargava, S. K., Hobday, M., and Foger, K., *J. Catal*. **158**, 301 (1996).
38. Akolekar, D. B., Bhargava, S. K., and Foger, K., *J. Chem. Soc., Faraday Trans*. **94**, 155 (1998).
39. Hadjiivanov, K., and Dimitrov, L., *Microporous Mesoporous Mater*. **27**, 49 (1999).
40. Henriques, C., Ribeiro, M. F., Abreu, C., Murphy, D. M., Poignant, F., Saussey, J., and Lavalley, J. C., *Appl. Catal. B* **16**, 79 (1998).
41. Dedecek, J., Sobalik, Z., Tvaruzkova, Z., Kaucky, D., and Wichterlowa, B., *J. Phys. Chem*. **99**(16), 327 (1995).
42. Hadjiivanov, K., Saussey, J., Freysz, J. L., and Lavalley, J. C., *Catal. Lett*. **52**, 103 (1998).
43. Hadjiivanov, K., *Catal. Rev.–Sci. Eng*. **42**, 71 (2000).
44. Morrow, B. A., McFarlane, R. A., Lion, M., and Lavalley, J. C., *J. Catal*. **107**, 232 (1987).
45. Bensitel, M., Waqif, M., Saur, O., and Lavalley, J. C., *J. Phys. Chem*. **93**, 6581 (1989).
46. Busca, G., *Catal. Today* **41**, 191 (1998).
47. Daturi, M., Binet, C., Lavalley, J. C., Galtayries, A., and Sporken, R., *Phys. Chem. Chem. Phys.* **1**, 5717 (1999).